



# A Novel Worm-like In-Pipe Robot with the Rigid and Soft Structure

Delei Fang<sup>1</sup> · Guofeng Jia<sup>1</sup> · Junran Wu<sup>1</sup> · Xiaoru Niu<sup>2</sup> · Pan Li<sup>1</sup> · Rong Wang<sup>3</sup> · Yan Zhang<sup>1</sup> · Junxia Zhang<sup>1</sup>

Received: 30 December 2022 / Revised: 4 May 2023 / Accepted: 7 May 2023 / Published online: 13 June 2023  
© Jilin University 2023

## Abstract

Soft in-pipe robot has good adaptability in tubular circumstances, while its rigidity is insufficient, which affects the traction performance. This paper proposes a novel worm-like in-pipe robot with a rigid and soft structure, which not only has strong traction ability but also flexible mobility in the shaped pipes. Imitating the structure features of the earthworm, the bionic in-pipe robot structure is designed including two soft anchor parts and one rigid telescopic part. The soft-supporting mechanism is the key factor for the in-pipe robot excellent performance, whose mathematical model is established and the mechanical characteristics are analyzed, which is used to optimize the structural parameters. The prototype is developed and the motion control strategy is planned. Various performances of the in-pipe robot are tested, such as the traction ability, moving velocity and adaptability. For comparative analysis, different operating scenarios are built including the horizontal pipe, the inclined pipe, the vertical pipe and other unstructured pipes. The experiment results show that the in-pipe robot is suitable for many kinds of pipe applications, the average traction is about 6.8N, the moving velocity is in the range of 9.5 to 12.7 mm/s.

**Keywords** In-pipe robot · Bionic design · Rigid and soft structure · Mechanical characteristics

## 1 Introduction

With the development of robotics and new materials, soft in-pipe robot having great advantages in complex environments has become a research hotspot [1, 2]. Compared with kinds of rigid in-pipe robots, the soft in-pipe robot mostly uses a crawling movement, imitating the motion mechanism of worms in nature [3–6]. The soft in-pipe robot can realize the movement in horizontal pipe, vertical pipe, multi-size pipe and other shaped pipe, which has a wide range of applications, especially in the industrial field of small and medium-sized pipe [7–9].

In recent years, more and more researchers have applied soft material science and technology to robotics [10–13]. For

the worm-like in-pipe robot, the soft-supporting mechanism directly affects its overall structure and output performance [14, 15]. Therefore, the research on soft-supporting characteristics and drive performance becomes significant [16–18]. Calderón A performed a pressure-strain test on a radial actuator for a multi-drive soft robot [19], whose result showed that there is some hysteresis behavior in the expansion to support the inner wall of the pipe. Dai proposed a worm-like tensegrity robot for in-pipe locomotion, which is capable of body deformation in the axial and radial directions under simple actuation. The proposed robot not only has a simple structure, lightweight but also has high compliance and adaptability [20]. Zhou developed a new pneumatic-driven earthworm-like soft robot, which achieves the robot's contacts with the external environment by means of three unidirectional crawling feet [21]. Zhang proposed a worm-like soft robot for complicated environments [22], which can support the body inside a wet, smooth or highly elastic tubular environment by sucking the module. Alcaide J O designed a flexible three-module robot that achieves contacting and supporting in tubular environments by pulling the skin expansion driven by a shape memory alloy, the passive resilience is produced by a new silicone skin with three cavities [23, 24]. Zhang designed the forefoot and hindfoot with a certain number of grooves to provide anchoring force for

✉ Delei Fang  
fangdelei@tust.edu.cn

<sup>1</sup> Tianjin Key Laboratory of Integrated Design and On-Line Monitoring for Light Industry & Food Machinery and Equipment, College of Mechanical Engineering, Tianjin University of Science and Technology, Tianjin 300222, China

<sup>2</sup> The Key Laboratory of Bionic Engineering, Ministry of Education, Jilin University, Changchun 130022, China

<sup>3</sup> National Institute of Innovation, Academy of Military Sciences, Beijing 100026, China

the robot in the pipe [25, 26]. Liu achieved uniform contacting and supporting with the pipe wall by Radial Expansion Pneumatic Actuators (REPAs) with four annular independent chambers [27]. Ishikawa designed the creeping crawling robot applying the radial expansion of artificial muscles [28]. Bernth investigated a worm-like robot with a body made of Polyethylene Terephthalate (PET) mesh material that could achieve anchoring support in tubular environments [29].

Although many researchers have developed a variety of soft structural in-pipe robots, theoretical research on supporting and driving is still rare. And the experiments show that if the robot is composed entirely of soft materials, the overall performance is limited. This paper does some work in the above two aspects, whose contributions are as follows. (1) By imitating earthworm creatures, a novel worm-like in-pipe robot with a rigid and soft structure is designed, which can be applied in an irregular tubular environment. (2) The mathematical model of the soft-supporting mechanism is established to analyze its mechanical characteristic and guide optimization of structural parameters. (3) The different experiments and the corresponding test methods are designed to study the robot's traction ability and flexible mobility.

The paper is organized as follows. In Sect. 2, the structure of the worm-like in-pipe robot is introduced. In Sect. 3, mathematical model for the robot is presented and the structural parameters are selected. Section 4 provides a description of the prototype and the experiments. In the experiments, it is shown that the robot cannot only move stably and quickly but also has high flexibility in complex tubular environments.

## 2 Bionic Idea and Structural Design

The proposed worm-like in-pipe robot is inspired by the soft structure and the peristaltic motion of the earthworm, which is shown in Fig. 1. In the initial state earthworm remain stationary, the head, body and tail anchor to the surroundings. At the next moment, the earthworm's body segments extend axially, causing the head to move forward. After that, the head of the earthworm is fixed in radial support, the body segments shrink axially, and the tail moves forward. Based on the above actions, the earthworm can move some distance and return to its original state. Repeating these above steps, the earthworm achieves continuous motion.

In this paper, a new type of worm-like in-pipe robot with a rigid and soft structure is proposed. Figure 2a shows the overall structure of the robot, which has two anchor parts at both ends and one telescopic part in the middle. The anchor part is Soft-Supporting Mechanism (SSM) which can anchor to the surroundings and the telescopic part is named Telescopic Mechanism (TM) which realizes the extension and

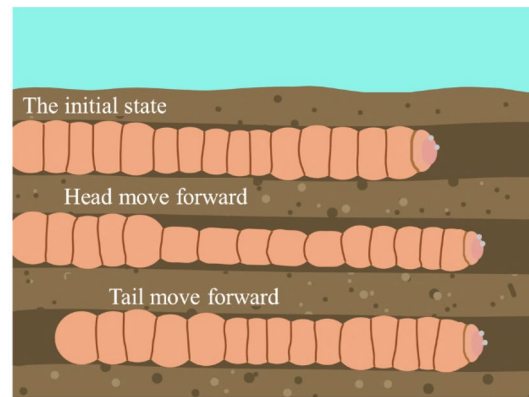


Fig. 1 The forward motion of the earthworm

retraction of the robot rigid body. The novel robot with rigid and soft structure has better performance than the conventional in-pipe robots [30–32]. The rigid structure provides strong traction capacity with high stiffness, and the soft structure can smoothly anchor the surroundings in complex pipes, such as bent pipes, reduced diameters pipes and obstructed pipes.

Figure 2b is the structural cross-sectional view. The SSM is mainly composed of the end cap, cartridge-shaped airbag and fastening strap. The end cap is provided with different channels to realize the arrangement of different gas circuits, to supply pressed air to the SSM and the TM. The structures of the end cap vary slightly according to the front position and the rear position. The TM mainly includes a pin cylinder (SMC-CJPB10-15), which has an inner diameter of 10 mm. The cylinder can output a theoretical force of 17.6N under 0.3 MPa air pressure. By controlling the inlet and outlet-pressed air of the SSM and the TM through solenoid valves, the in-pipe robot can realize fast and continuous motion. It is worth noting that the outer diameter and axial length of the TM are smaller than those of the SSM, which is always in suspension during the robot motion. Therefore, considering the pipe size and robot structure, the reasonable rigid telescopic mechanism will not affect the passive compliance of the robot. In addition, according to the different application requirements, the series design based on the robot's basic mechanism is possible.

## 3 Analysis of Soft-Supporting Mechanism

### 3.1 Anchoring Condition

The maximum static friction force on the Soft-Supporting Mechanism is the decisive factor for the worm-like in-pipe robot to move normally in an irregular environment. So, it

**Fig. 2** Diagram of the worm-like in-pipe robot structure: **a** the overall structural; **b** structural cross-sectional view

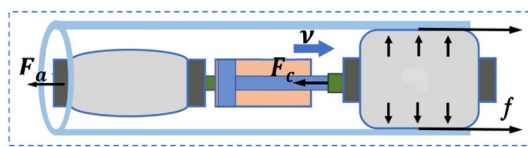
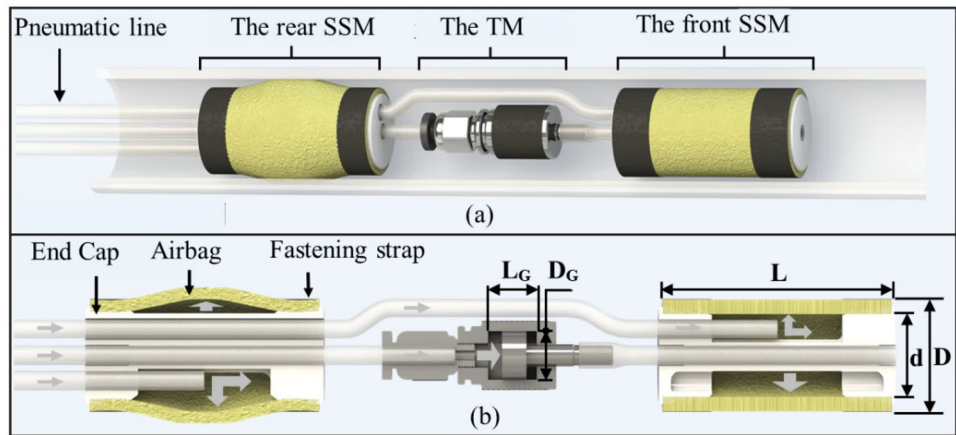


**Fig. 3** Diagram of forces on the in-pipe robot

is necessary to analyze the maximum static friction force on the SSM and work out the anchoring conditions.

Select a movement moment of the robot to carry on the force analysis, shown in Fig. 3. Set the maximum load to  $F_w$ , the robot itself generates a load  $F_a$ , and the robot's maximum traction is  $F_{c\max}$ . The load equation of the robot is obtained.

$$F_w = F_a + F_{c\max} = F_a + \frac{\pi D_G^2 P_G}{4} \tag{1}$$

where  $D_G$  is the piston diameter of the telescoping cylinder,  $P_G$  is the air pressure injected into the cylinder, and  $F_a$  is the component of the robot's gravity, which depends on the tilt angle of the pipe.

The maximum static friction force on the front SSM can be expressed as follows.

$$f_{\max} = \mu F_N = \mu P \pi D_p L_S \tag{2}$$

where  $\mu$  is the friction coefficient between the front SSM and inner wall of the pipe,  $D_p$  is the inner diameter of the pipe,  $L_S$  is the contact length between the airbag and the pipe, and  $P$  is the air pressure injected into the front airbag.

The following conditions must be met for the stable movement of the robot.

$$f_{\max} \geq F_w \tag{3}$$

Combine formula 1, 2 and 3 to get formula 4.

$$L_S \geq \frac{1}{\mu P \pi D_p} \left( F_a + \frac{\pi D_G^2 P_G}{4} \right) \tag{4}$$

Therefore, the condition that the robot can walk normally should meet the requirements in formula 4.

### 3.2 Mathematical Model

The airbag used in the Soft-Supporting Mechanism is made of elastic material, which has nonlinear properties. As the Yeoh model is suitable for the mathematical model of large deformation on the nonlinear materials, and its model form is simple and sufficiently accurate, the Yeoh model is chosen to describe the mathematical model of the airbag.

Supposing the airbag material is isotropic, based on the Mooney-Rivlin ontological model, the density function of strain energy  $W$  is obtained. Where  $I_1, I_2$  and  $I_3$  are deformation tensor invariants,  $\lambda_1, \lambda_2$  and  $\lambda_3$  are axial drawing ratio, radial drawing ratio and circumferential drawing ratio. Some relations are obtained.

$$W = W(I_1, I_2, I_3) \tag{5}$$

$$I_1 = \lambda_1^2 + \lambda_2^2 + \lambda_3^2 \tag{6}$$

$$I_2 = \lambda_1^2 \lambda_2^2 + \lambda_2^2 \lambda_3^2 + \lambda_3^2 \lambda_1^2 \tag{7}$$

$$I_3 = \lambda_1^2 \lambda_2^2 \lambda_3^2 \tag{8}$$

As the incompressibility of rubber material,  $I_3 = 1$ . For simplicity of calculation, the radial drawing ratio is 1. So, the following system is obtained.

$$\begin{cases} \lambda_3 = \frac{1}{\lambda_1} \\ I_1 = \lambda_1^2 + \frac{1}{\lambda_1^2} + 1 \end{cases} \quad (9)$$

Based on the binomial form of the Yeoh model, the density function model of strain energy is got.

$$W = C_1(I_1 - 3) + C_2(I_1 - 3)^2 \quad (10)$$

where  $C_1$  and  $C_2$  are material constants, and the final simplification is obtained.

$$W = C_1 \left( \lambda_1^2 + \frac{1}{\lambda_2} - 2 \right) + C_2 \left( \lambda_1^2 + \frac{1}{\lambda_2} - 2 \right)^2 \quad (11)$$

Based on the formula (11), the characteristics of soft-supporting can be analyzed. By studying the relationship between the maximum expansion of the airbag and the air pressure, the diameters range of the applicable pipe for the worm-like in-pipe robot can be obtained. In addition, the optimal dimension parameters of the SSM can also be selected, which provides the basis for the development of the robot prototype.

### 3.3 Parameter Selection

The Yeoh model of Eq. (11) is used to describe the rubber material of the airbag, where the material parameters are initially selected as  $C_1 = 0.11$ ,  $C_2 = 0.02$ . The outer diameter of the airbag is set to  $D = 20$  mm, which can meet the requirement for the pipe diameters ranging from 25 to 40 mm. The influences of airbag length  $L$  and airbag inner diameter  $d$  on the soft-supporting performance is analyzed below.

Figure 4 shows the effect of airbag length on the soft-supporting characteristics when the initial parameter of the airbag is 15 mm as the inner diameter and 20 mm as the outer diameter. It can be seen that the expansion of the airbag increases with the increase of air pressure. Under the same air pressure, the longer the airbag length is, the larger the airbag expansion is. While, when the air pressure ranges from 0.05 MPa–0.15 MPa, the maximum expansion of 50 mm, 60 mm and 70 mm length of the airbag is basically the same, and the expansion of 70 mm length reaches its limitation on the pressure of 0.15 MPa. There are two considerations when the airbag length is selected: (1) to pursue the larger static friction force, the airbag length should be larger, (2) to improve the flexibility of the robot, the airbag length should be smaller. Considering the above two aspects, the length of the airbag is preferably 50 mm.

Figure 5 shows the effect of different inner diameters of the airbag on the soft-supporting characteristics when the length of the airbag is 50 mm.

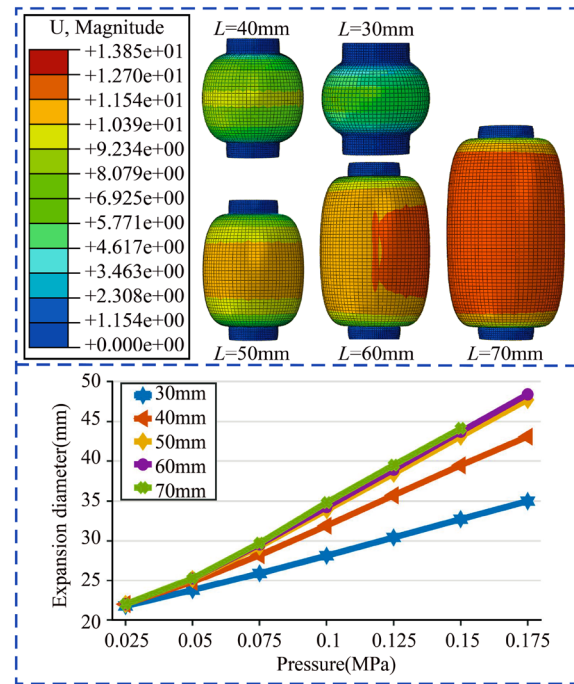


Fig. 4 Characteristics effect of different airbag length

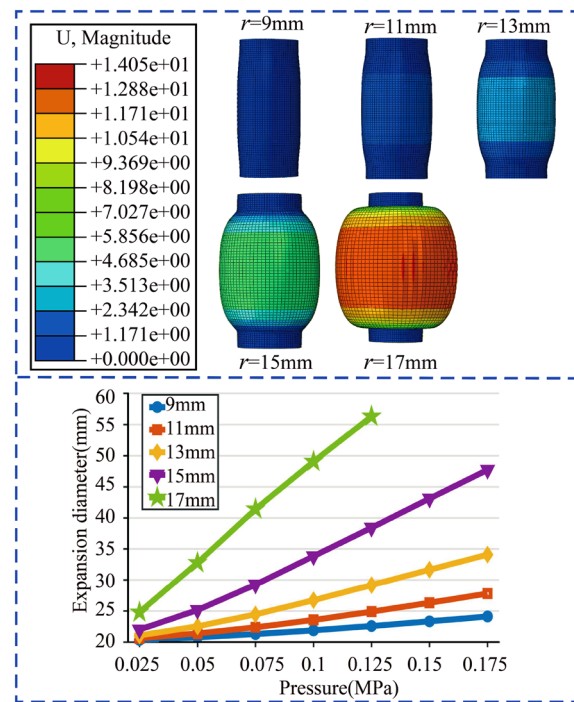
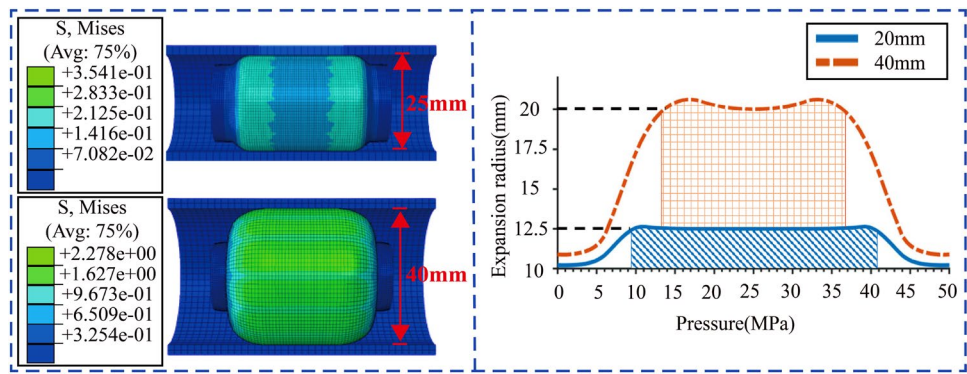


Fig. 5 Characteristics effect of different inner diameters

Generally, the expansion of the airbag increases with the increase of the airbag inner diameter. What is more, the increase of the airbag with a larger inner diameter is more significant than that with a smaller inner diameter. When the

**Fig. 6** Simulation of the SSM with the selected parameters



**Table 1** The main parameters of the worm-like in-pipe robot

Parameters	Values
$\mu$	0.2
$F_a$	10N
$D_G$	10 mm
$P_G$	0.6 MPa

air pressure is 0.125 MPa, the airbag with an inner diameter of 17 mm reaches the expansion limitation. According to the working requirements, airbags with inner diameters of 9 mm, 11 mm and 13 mm are firstly excluded, and the airbag with an inner diameter of 17 mm has a thinner wall which is liable to be damaged, so the airbag with an inner diameter of 15 mm is selected finally.

After the above analysis, the airbag length  $L = 50$  mm, the airbag inner diameter  $d = 15$  mm and the airbag outer diameter  $D = 20$  mm are selected as the final dimensions of the SSM. Simulation is conducted and the result is shown in Fig. 6. When SSM anchors to the inner wall of the pipe with 25 mm diameter, the effective contact area between the airbag and the pipe wall reaches the maximum value (the air pressure is 0.125 MPa). When the SSM anchors to the inner wall of the pipe with a 40 mm diameter, the effective contact area reaches the maximum value (the air pressure is 0.175 MPa). The above data provide good theoretical guidance for the traction force output of the worm-like in-pipe robot.

The specific effective contact data between the SSM and the inner wall of the pipe are obtained as follows. For the inner diameters of 25 mm and 40 mm, the effective contact distances are  $L_{S25} = 32$  mm and  $L_{S40} = 24$  mm, respectively, and other parameters are shown in Table 1.

Specific parameters can be substituted into formula (4) to verify whether the motion of the worm-like in-pipe robot is reliable finally.

$$L_{S25} = 32 \text{ mm} \geq \frac{F_a + \frac{\pi D_G^2 P_G}{4}}{\mu P_{25} \pi D_{P25}} = 29.09 \text{ mm} \quad (12)$$

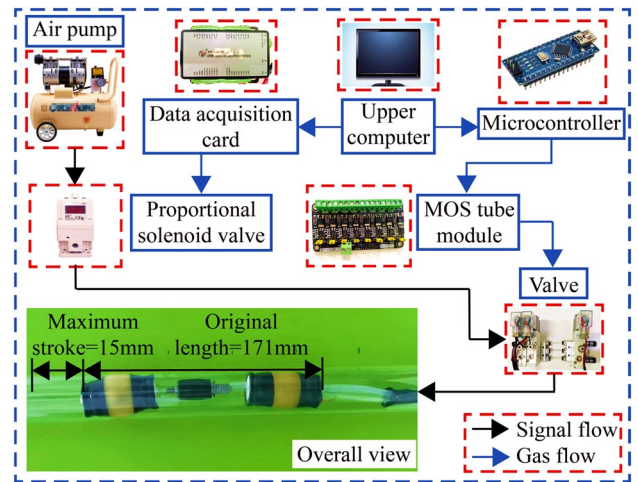


**Fig. 7** Overall view of prototype and test system

$$L_{S40} = 24 \text{ mm} \geq \frac{F_a + \frac{\pi D_G^2 P_G}{4}}{\mu P_{40} \pi D_{P40}} = 12.9 \text{ mm} \quad (13)$$

It can be seen from the above formulas that the selected parameters of the rubber airbag meet the design requirements for the robot. With these parameters, the novel in-pipe robot will demonstrate excellent traction ability and adaptation performance.

## 4 Experiment and Discussion

### 4.1 Test System

The worm-like in-pipe robot prototype is developed, with an original length of 171 mm and a maximum stoke of 10 mm, which is shown in Fig. 7.

The test system includes the drive system which provides the robot power and the control system which controls the robot's motion. The drive system contains an air pump, proportional valve and some direction valves. The control

system consists of an upper computer, microcontroller, data acquisition card and MOS modules.

Imitating the principle of the earthworm’s continuous motion, a gait control strategy is presented to realize the flexible movement of the in-pipe robot. Figure 8a shows 6 steps in one motion cycle, and Fig. 8b reveals the different states of each mechanism.

Step 1: Both the front SSM and the rear SSM remain inflated (ON state) and anchor to the inner wall of the pipe, the telescopic mechanism is deflated (OFF state).

Step 2: The front SSM becomes deflated (OFF state), and the rear SSM remains inflated (ON state).

Step 3: The telescopic mechanism becomes inflated (ON state) and pushes the front SSM move forward.

Step 4: The front SSM is inflated (ON state) to anchor the inner wall of the pipe.

Step 5: The rear SSM deflates (OFF state) and detaches from the inner wall of the pipe.

Step 6: The telescopic mechanism is deflated (OFF state) and retracted to its original length. The robot completes one cycle and move forward with the length  $L$ .

### 4.2 Traction Ability Test

The relationship between airbag expansion and gas pressure is tested before the robot traction ability test. Experiments are conducted in both pipe-bound and pipe-free environments, the results are plotted as shown in Fig. 9. The expansion of the airbag increases linearly with the increase of gas pressure in the initial stage. When the gas pressure reached 0.08 MPa, the airbag with pipe-free begin to expand rapidly and eventually ruptured. The airbag under the constraint of the pipe does not rupture and finally contact with the pipe’s inner wall. As the gas pressure increases, the contact area between the airbag and the pipe continues to increase. The expansion diameter of the airbag reached a range of

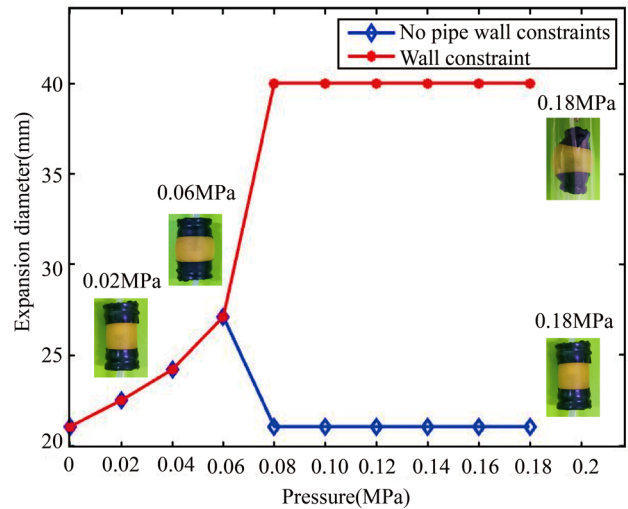


Fig. 9 Relationship between airbag expansion and gas pressure

25–40 mm, and the larger deformation could improve the robot’s adaptability.

The experimental platform was used to test the supporting force of the SSM in the pipe with an inner diameter of 30 mm. Figure 10a shows the relationship between the supporting force and the air pressure. With the increase of air pressure, the supporting force gradually increases. The maximum supporting force is stable at 67.2N when the pressure reaches 0.18 MPa, which makes a strong guarantee for the large traction of the robot.

Figure 11 shows the experimental test rig for the robot’s traction ability. the robot is placed inside a pipe and its tail is connected to the force transducer (ARIZON AR-DN103 200N), which is fixed on the holder. The gas pressure is controlled by the proportional valve.

Test the robot output traction where obstacles are arranged in the pipe or not and draw the curves which is

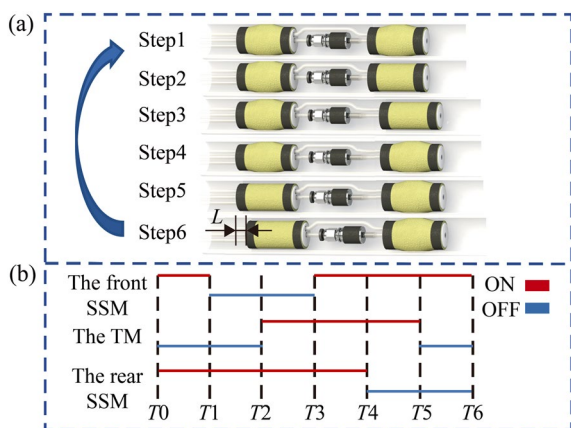


Fig. 8 Gait control strategy in a motion cycle: a steps of a motion cycle; b different states of each mechanism

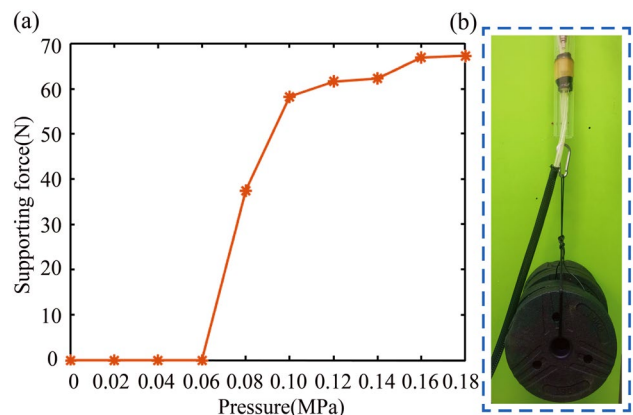


Fig. 10 Supporting force experiment: a the force curve, b the experimental arrangement

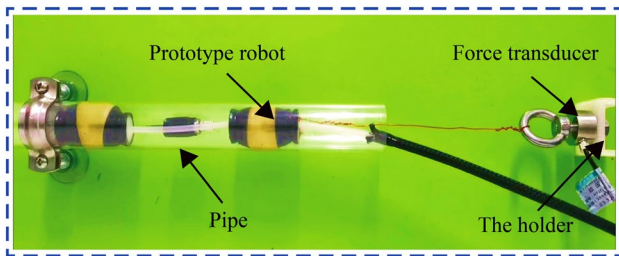


Fig. 11 Experimental test rig for traction

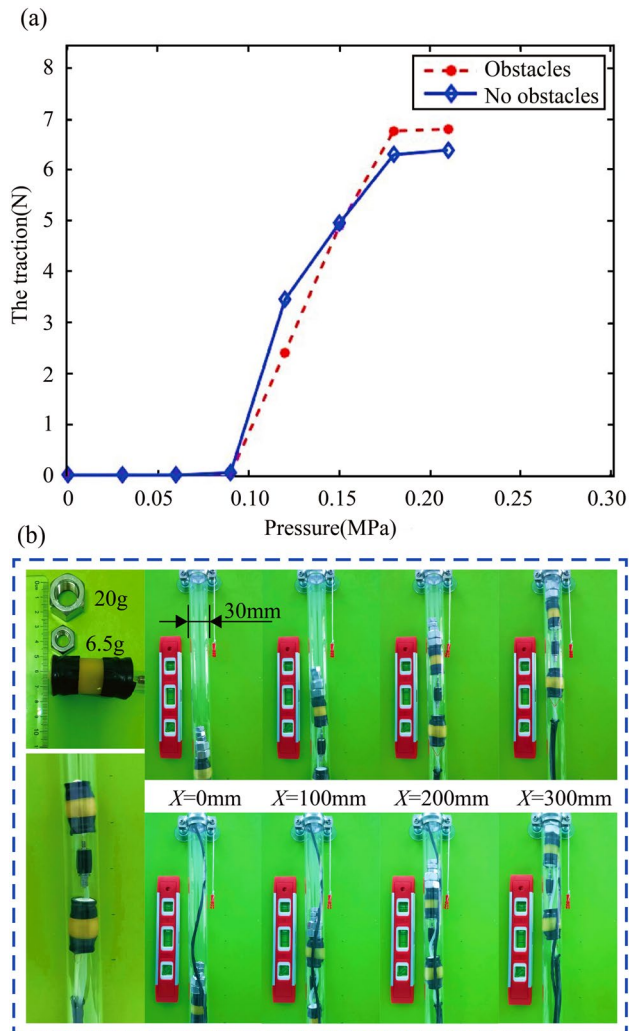


Fig. 12 Traction experiment: **a** traction curves, **b** the robot motions in different pipe walls

shown in Fig. 12a. When the air pressure is lower than 0.08 MPa, the robot cannot move due to the insufficient anchoring of the soft-supporting mechanism. When the motion condition is met, the robot output traction increases with the increase of air pressure until it reaches a stable

value at 0.17 MPa. As can be seen from Fig. 12a, whether there are obstacles in the pipe has little influence on the robot's traction, which maintains a stable traction of 6.8N, which demonstrates the powerful adaptation ability in a complex environment of this novel in-pipe robot based on soft-supporting mechanism. In addition, in Fig. 12b, the motion states of the robot prove that the crawling ability of the pipe robot is not greatly affected although it is hung in different loads in kinds of pipes.

### 4.3 Moving Velocity

To explore the effect of robot moving velocity in different directional pipes, we select kinds of arrangement for the pipe. Figure 13a shows the robot motion in a 30 mm diameter pipe. The air pressure is set to 0.153 MPa, and the velocity experiment is conducted in the horizontal pipe, the inclined pipe and the vertical pipe.

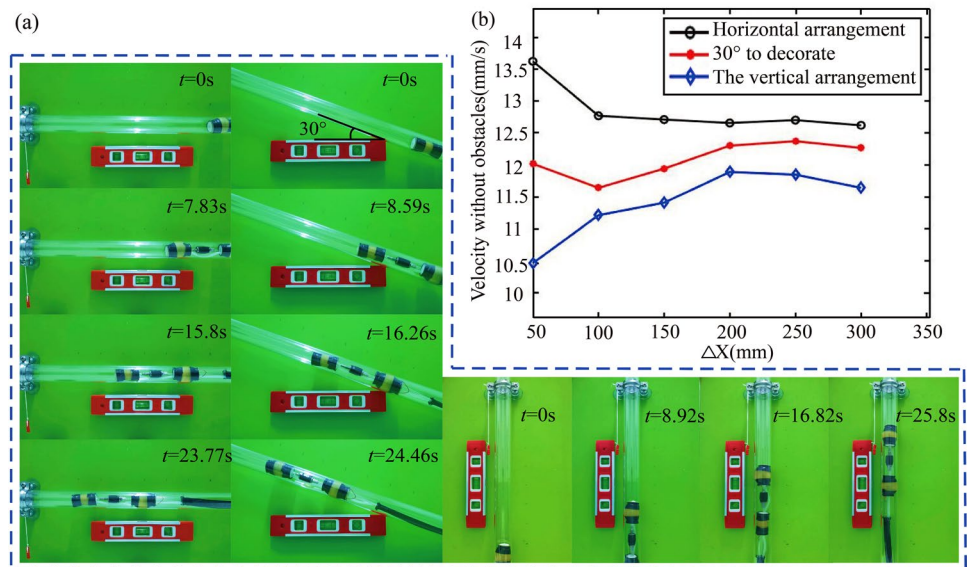
As can be seen from Fig. 13b, the robot's horizontal moving speed gradually keeps a steady velocity of 12.7 mm/s, and there is no much difference compared with the moving speed in the 30° inclined pipe and in the vertical pipe, which are basically stable in the range of 11.5 mm/s-13 mm/s. It indicates that the robot's moving velocity is less influenced by different angles of pipe arrangement.

Figure 14a shows the robot moving velocity experiment with obstacles, and the other experimental conditions are the same as the test experiment without obstacles. From Fig. 14b, it can be seen that the robot moves at the highest speed and fluctuates about 12.3 mm/s in the vertical pipe, the velocity of the 30° inclined pipe is lower by 10 mm/s, and the velocity in the horizontal pipe is lowest by 9.5 mm/s. According to the analysis, the movement of the robot is affected by the friction resistance caused by obstacles. The robot moves in the vertical pipe with the least friction resistance, so it moves at the highest speed. While the robot moves in the horizontal pipe, the friction resistance is the highest, so the movement speed is the lowest.

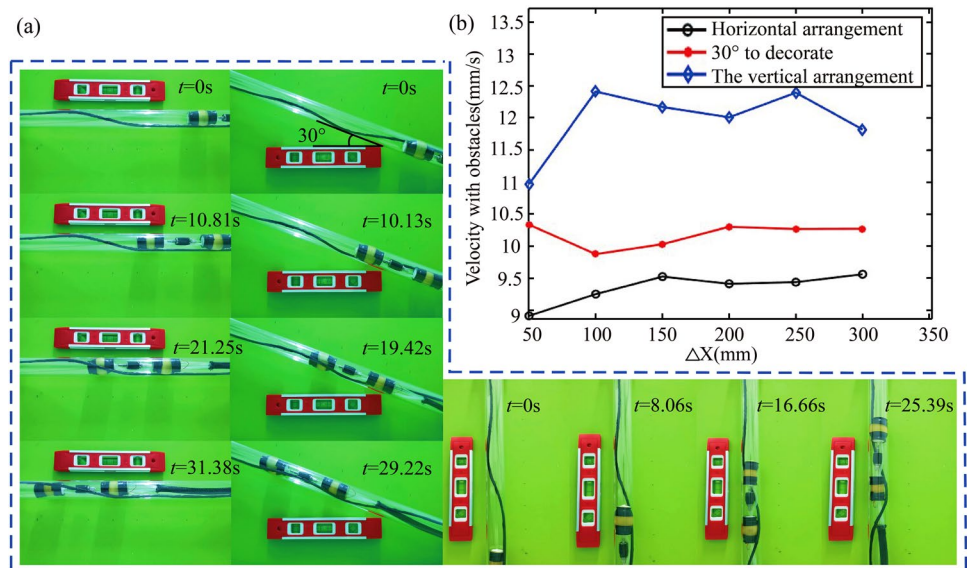
By summarizing the experiment results of Figs. 13 and 14, it can be seen that the moving velocity of the in-pipe robot is maintained at 9.5 mm/s-12.7 mm/s, although in a different pipe environment. The above finding can indicate that the in-pipe robot based on SSM can stably anchor the pipe in various conditions and output an efficient moving velocity.

Table 2 lists some classical robots in the same size structure that have been developed in recent decades [23, 33–35]. The No.5 robot is the prototype developed in this paper, which shows the great advantages in adapting to the pipe diameter range, traction capacity and running speed.

**Fig. 13** Velocity in kinds of pipes: **a** in a horizontal pipe, in the inclined pipe, in the vertical pipe; **b** different moving velocity curves



**Fig. 14** moving velocity experiment with obstacles: **a** motion in a horizontal pipe, the 30° inclined pipe and the vertical pipe, **b** different moving velocity curves



**Table 2** The main parameters of the worm-like in-pipe robot

No	Type	Diameter (mm)	Traction (N)	Velocity (mm/s)
1 [33]	Rigid	24–25	1	6
2 [34]	Rigid	14–20	3.58	1.3
3 [23]	Soft	24–40	4	4
4 [35]	Soft	15–27	4.7	1.3
5	Rigid-soft	25–40	6.8	12.7

### 4.4 Unstructured Environment

Because of the pneumatic drive and soft-supporting structure, the worm-like in-pipe robot can operate in

unstructured environments. Figure 15a shows the motion of the robot in a U-shaped pipe with a curvature radius of 90 mm. The robot moves in the tube stably. Figure 15b shows the robot motion in a U-shaped pipe filled with water. The in-pipe pipe robot also achieves a 90-degree turning motion. As the difference in static friction force, the moving speed in water is slightly slower than that in a dry pipe. Figure 16a and Fig. 16b show the robot moving in a non-circular pipe. The pipe robot can crawl forward smoothly by modifying the round pipe into a fan-shaped pipe and the oval pipe. While, these above results have provided strong proof that this type of worm-like in-pipe robot can work normally in such an unstructured environment, and we get the tips that the in-pipe robot operates in the fluid pipe, the material of the soft airbag needs





**Fig. 15** motion experiment in an unstructured environment **a** motion in a U-pipe, **b** motion in a U-pipe filled with water

attention, which is the key factor for the friction force between the robot and the pipe wall.

## 5 Conclusion

A novel worm-like in-pipe robot with a rigid and soft structure is presented in this paper, which has strong traction ability and flexible mobility in complex shape pipes.

Imitating the soft structure and motion mode of the earthworm, the bionic robot structure was designed and the motion strategy was formulated. Based on the theoretical analysis, the movement conditions and the mathematical model were established, and the mechanical characteristics of the Soft-Supporting Mechanism were analyzed. Finally, the robot's prototype was developed and performance tests are completed, including traction ability, moving velocity and adaptability in the unstructured environments, which showed that the average traction ability is about 6.8N, the moving velocity is stable in the range of 9.5 mm/s–12.7 mm/s, and the robot is suitable for kinds of pipe applications. The above research work provides a good reference for the theoretical analysis and experimental test of soft in-pipe robot.



**Fig. 16** non-round pipe experiments: **a** fan-shaped pipe, **b** oval pipe

**Funding** National Natural Science Foundation of China, 52005369, Open Project Fund of Tianjin Key Laboratory of Integrated Design and Online Monitoring of Light Industry and Food Engineering Machinery and Equipment, 2020LIMFE05.

**Data availability** The data that support the findings of this study are available from the corresponding author upon reasonable request.

## Declarations

**Conflict of interest** The authors declare that they have no known competing financial interests or personal relationships that could have appeared to influence the work reported in this paper.

## References

- Chen, G., Yang, X., Xu, Y., Lu, Y., & Hu, H. (2022). Neural network-based motion modeling and control of water-actuated soft robotic fish. *Smart Materials and Structures*, 32(1), 015004. <https://doi.org/10.1088/1361-665X/aca456>
- Shao, L., Wang, Y., Guo, B., & Chen, X. (2015). A review over state of the art of in-pipe robot. *The Proceedings of IEEE International Conference on Mechatronics and Automation (ICMA)*, Beijing, China, 2180–2185, <https://doi.org/10.1109/ICMA.2015.7237824>

3. Chen, G., Lu, Y., Yang, X., & Hu, H. (2022). Reinforcement learning control for the swimming motions of a beaver-like, single-legged robot based on biological inspiration. *Robotics and Autonomous Systems*, 154, 104116. <https://doi.org/10.1016/j.robot.2022.104116>
4. Ismail, I. N., Anuar, A., Sahari, K. S. M., Baharuddin, M. Z., Fairuz, M., Jalal, A., & Saad, J. M. (2012). Development of in-pipe inspection robot: a review. *The Proceedings of Conference on Sustainable Utilization and Development in Engineering and Technology (STUDENT)*, Kuala Lumpur, Malaysia 310–315, <https://doi.org/10.1109/STUDENT.2012.6408425>
5. Zhao, S., Yan, Z., Meng, Q., Xiao, H., Lai, X., & Wu, M. (2022). Modified three-element modeling and robust tracking control for a planar pneumatic soft actuator. *IEEE Transactions on Industrial Electronics*. <https://doi.org/10.1109/TIE.2022.3206693>
6. Xu, Z. L., Lu, S., Yang, J., Feng, Y. H., & Shen, C. T. (2017). A wheel-type in-pipe robot for grinding weld beads. *Advances in Manufacturing*, 5(2), 182–190. <https://doi.org/10.1007/s40436-017-0174-9>
7. Oka, Y., Kakogawa, A., & Ma, S. (2021). A wheeled v-shaped in-pipe robot with clutched underactuated joints. *The Proceedings of IEEE International Conference on Robotics and Automation (ICRA)*, Xi'an, China, 11457–11462, <https://doi.org/10.1109/ICRA48506.2021.9561775>
8. Winstone, B., Pipe, T., Melhuish, C., Callaway, M., Etoundi, A. C., & Dogramadzi, S. (2016). Single motor actuated peristaltic wave generator for a soft bodied worm robot. *The Proceedings of IEEE International Conference on Biomedical Robotics and Biomechatronics (BioRob)*, Singapore, 449–456, <https://doi.org/10.1109/BIOROB.2016.7523668>
9. Streich, H., & Adria, O. (2004). Software approach for the autonomous inspection robot makro. *The Proceedings of IEEE International Conference on Robotics and Automation (ICRA)*, New Orleans, LA, USA, 3411–3416, <https://doi.org/10.1109/ROBOT.2004.1308781>
10. Laschi, S. R., Mazzolai, B., & Cianchetti, M. (2016). Technologies and systems pushing the boundaries of robot abilities. *Science Robotics*, 1(1), 1–11. <https://doi.org/10.1126/scirobotics.aah3690>
11. Verma, M. S., Ainla, A., Yang, D., Harburg, D., & Whitesides, G. M. (2018). A soft tube-climbing robot. *Soft Robotics*, 5(2), 133–137. <https://doi.org/10.1089/soro.2016.0078>
12. Rus, D., & Tolley, M. T. (2015). Design, fabrication and control of soft robots. *Nature*, 521(7553), 467–475. <https://doi.org/10.1038/nature14543>
13. Kanada, A., Giardina, F., Howison, T., Mashimo, T., & Iida, F. (2019). Reachability improvement of a climbing robot based on large deformations induced by tri-tube soft actuators. *Soft Robotics*, 6(4), 483–494. <https://doi.org/10.1089/soro.2018.0115>
14. Polygerinos, P., Correll, N., Morin, S. A., Mosadegh, B., Onal, C. D., Petersen, K., & Shepherd, R. F. (2017). Soft robotics: Review of fluid-driven intrinsically soft devices; manufacturing, sensing, control, and applications in human-robot interaction. *Advanced Engineering Materials*, 19(12), 1700016. <https://doi.org/10.1002/adem.201700016>
15. Bao, G., Fang, H., Chen, L., Wan, Y., Xu, F., Yang, Q., & Zhang, L. (2018). Soft robotics: Academic insights and perspectives through bibliometric analysis. *Soft Robotics*, 5(3), 229–241. <https://doi.org/10.1089/soro.2017.0135>
16. Shi, Z., Pan, J., Tian, J., Huang, H., Jiang, Y., & Zeng, S. (2019). An inchworm-inspired crawling robot. *Journal of Bionic Engineering*, 16(4), 582–592. <https://doi.org/10.1007/s42235-019-0047-y>
17. Duduta, M., Clarke, D. R., & Wood, R. J. (2017). A high speed soft robot based on dielectric elastomer actuators. *The Proceedings of IEEE International Conference on Robotics and Automation (ICRA)*, Singapore, 4346–4351. <https://doi.org/10.1109/ICRA.2017.7989501>
18. Wu, P., Jiangbei, W., & Yanqiong, F. (2018). The structure, design, and closed-loop motion control of a differential drive soft robot. *Soft robotics*, 5(1), 71–80. <https://doi.org/10.1089/soro.2017.0042>
19. Calderón, A. A., Ugalde, J. C., Zagal, J. C., & Pérez-Arancibia, N. O. (2016). Design, fabrication and control of a multi-material-multi-actuator soft robot inspired by burrowing worms. *The Proceedings of IEEE International Conference on Robotics and Biomimetics (ROBIO)*, Qingdao, China, 31–38. <https://doi.org/10.1109/ROBIO.2016.7866293>
20. Dai, X., Liu, Y., Wang, W., Song, R., Li, Y., & Zhao, J. (2022). Design and experimental validation of a worm-like tensegrity robot for in-pipe locomotion. *Journal of Bionic Engineering*. <https://doi.org/10.1007/s42235-022-00301-1>
21. Zhou, X., Teng, Y., & Li, X. (2016). Development of a new pneumatic-driven earthworm-like soft robot. *The Proceedings of International Conference on Mechatronics and Machine Vision in Practice (M2VIP)*, Nanjing, China, 1–5, <https://doi.org/10.1109/M2VIP.2016.7827269>
22. Zhang, B., Fan, Y., Yang, P., Cao, T., & Liao, H. (2019). Worm-like soft robot for complicated tubular environments. *Soft robotics*, 6(3), 399–413. <https://doi.org/10.1089/soro.2018.0088>
23. Alcaide, J. O., Pearson, L., & Rentschler, M. E. (2017). Design, modeling and control of a sma-actuated biomimetic robot with novel functional skin. *The Proceedings of IEEE International Conference on Robotics and Automation (ICRA)*, Singapore, 4338–4345, <https://doi.org/10.1109/ICRA.2017.7989500>
24. Bian, S., Wei, Y., Xu, F., & Kong, D. (2021). A four-legged wall-climbing robot with spines and miniature setae array inspired by longicorn and gecko. *Journal of Bionic Engineering*, 18(2), 292–305. <https://doi.org/10.1007/s42235-021-0032-0>
25. Zhang, Z., Wang, X., Wang, S., Meng, D., & Liang, B. (2019). Design and modeling of a parallel-pipe-crawling pneumatic soft robot. *IEEE access*, 7, 134301–134317. <https://doi.org/10.1109/ACCESS.2019.2941502>
26. Zhang, Z., Wang, X., Liu, H., Liang, B., & Wang, S. (2018). Kinematic analysis of novel soft robotic arm based on virtual work principle. *The Proceedings of IEEE International Conference on Robotics and Biomimetics (ROBIO)* Kuala Lumpur, Malaysia, 984–990, <https://doi.org/10.1109/ROBIO.2018.8665169>
27. Liu, X., Song, M., Fang, Y., Zhao, Y., & Cao, C. (2022). Worm-inspired soft robots enable adaptable pipeline and tunnel inspection. *Advanced Intelligent Systems*, 4(1), 2100128. <https://doi.org/10.1002/aisy.202100128>
28. Ishikawa, R., Tomita, T., Yamada, Y., & Nakamura, T. (2016). Development of a peristaltic crawling robot for long-distance complex line sewer pipe inspections. *The Proceedings of International Conference on Advanced Intelligent Mechatronics (AIM)* Banff, AB, Canada, 413–418, <https://doi.org/10.1109/AIM.2016.7576802>
29. Bernth, J. E., Arezzo, A., & Liu, H. (2017). A novel robotic mesh-worm with segment-bending anchoring for colonoscopy. *IEEE Robotics and Automation Letters*, 2(3), 1718–1724. <https://doi.org/10.1109/LRA.2017.2678540>
30. Qiao, J., Shang, J., & Goldenberg, A. (2012). Development of inchworm in-pipe robot based on self-locking mechanism. *IEEE/ASME Transactions On Mechatronics*, 18(2), 799–806. <https://doi.org/10.1109/TMECH.2012.2184294>
31. Nakazato, Y., Sonobe, Y., & Toyama, S. (2010). Development of an in-pipe micro mobile robot using peristalsis motion. *Journal of Mechanical Science and Technology*, 24, 51–54. <https://doi.org/10.1007/s12206-009-1174-x>
32. Liu, K., Chen, W., Yang, W., Jiao, Z., & Yu, Y. (2022). Review of the research progress in soft robots. *Applied Sciences*, 13(1), 120. <https://doi.org/10.3390/app13010120>

33. Suzumori, K., Miyagawa, T., Kimura, M., & Hasegawa, Y. (1999). Micro inspection robot for 1-in pipes. *IEEE/ASME Transactions on Mechatronics*, 4(3), 286–292. <https://doi.org/10.1109/3516.789686>
34. Simi, M., Valdastrì, P., Quaglia, C., Menciassi, A., & Dario, P. (2010). Design, fabrication, and testing of a capsule with hybrid locomotion for gastrointestinal tract exploration. *IEEE/ASME Transactions on Mechatronics*, 15(2), 170–180. <https://doi.org/10.1109/TMECH.2010.2041244>
35. Heung, H., Chiu, P. W. Y., Li, Z. (2016). Design and prototyping of a soft earthworm-like robot targeted for gi tract inspection, *The Proceedings of IEEE International Conference on Robotics and*

*Biomimetics (ROBIO)*, Qingdao, China, 497–502. <https://doi.org/10.1109/ROBIO.2016.7866371>

**Publisher's Note** Springer Nature remains neutral with regard to jurisdictional claims in published maps and institutional affiliations.

Springer Nature or its licensor (e.g. a society or other partner) holds exclusive rights to this article under a publishing agreement with the author(s) or other rightsholder(s); author self-archiving of the accepted manuscript version of this article is solely governed by the terms of such publishing agreement and applicable law.